Research Article | Vol. 26, No. 10 | 14 May 2018 | OPTICS EXPRESS 12506
Optics EXPRESS

102 fs pulse generation from a long-term stable, inkjet-printed black phosphorus-mode-locked fiber laser

XINXIN JIN,[1,4] GUOHUA HU,[2,4] MENG ZHANG,[1,*] YUWEI HU,[1] TOM ALBROW-OWEN,[2] RICHARD C. T. HOWE,[2] TIEN-CHUN WU,[2] QING WU,[1] ZHENG ZHENG,[1,3] AND TAWFIQUE HASAN[2]

[1]*School of Electronic and Information Engineering, Beihang University, Beijing, 100191, China*
[2]*Cambridge Graphene Centre, University of Cambridge, Cambridge, CB3 0FA, UK*
[3]*Collaborative Innovation Center of Geospatial Technology, Wuhan, 430079, China*
[4]*These authors contributed equally to this work*
**mengzhang10@buaa.edu.cn*

Abstract: We demonstrate a long-term stable, all-fiber, erbium-doped femtosecond laser mode-locked by a black phosphorus saturable absorber. The saturable absorber, fabricated by scalable and highly controllable inkjet printing technology, exhibits strong nonlinear optical response and is stable for long-term operation against intense irradiation, overcoming a key drawback of this material. The oscillator delivers self-starting, 102 fs stable pulses centered at 1555 nm with 40 nm spectral bandwidth. This represents the shortest pulse duration achieved from black phosphorus in a fiber laser to date. Our results demonstrate the great potential for black phosphorus as an excellent candidate for long-term stable ultrashort pulse generation.

© 2018 Optical Society of America under the terms of the OSA Open Access Publishing Agreement

OCIS codes: (140.3510) Lasers, fiber; (140.7090) Ultrafast lasers; (160.4236) Nanomaterials.

References and links

1. K. Tamura, E. P. Ippen, H. A. Haus, and L. E. Nelson, "77-fs pulse generation from a stretched-pulse mode-locked all-fiber ring laser," Opt. Lett. **18**(13), 1080–1082 (1993).
2. D. Y. Tang and L. M. Zhao, "Generation of 47-fs pulses directly from an erbium-doped fiber laser," Opt. Lett. **32**(1), 41–43 (2007).
3. D. Popa, Z. Sun, T. Hasan, W. B. Cho, F. Wang, F. Torrisi, and A. C. Ferrari, "74-fs nanotube-mode-locked fiber laser," Appl. Phys. Lett. **101**(15), 4 (2012).
4. Z. P. Sun, T. Hasan, F. Q. Wang, A. G. Rozhin, I. H. White, and A. C. Ferrari, "Ultrafast stretched-pulse fiber laser mode-locked by carbon nanotubes," Nano Res. **3**(6), 404–411 (2010).
5. X. Li, W. Zou, and J. Chen, "41.9 fs hybridly mode-locked Er-doped fiber laser at 212 MHz repetition rate," Opt. Lett. **39**(6), 1553–1556 (2014).
6. Y. W. Song, S. Y. Jang, W. S. Han, and M. K. Bae, "Graphene mode-lockers for fiber lasers functioned with evanescent field interaction," Appl. Phys. Lett. **96**(5), 183 (2010).
7. G. Sobon, J. Sotor, I. Pasternak, A. Krajewska, W. Strupinski, and K. M. Abramski, "All-polarization maintaining, graphene-based femtosecond Tm-doped all-fiber laser," Opt. Express **23**(7), 9339–9346 (2015).
8. W. Liu, L. Pang, H. Han, M. Liu, M. Lei, S. Fang, H. Teng, and Z. Wei, "Tungsten disulfide saturable absorbers for 67 fs mode-locked erbium-doped fiber lasers," Opt. Express **25**(3), 2950–2959 (2017).
9. J. Du, M. Zhang, Z. Guo, J. Chen, X. Zhu, G. Hu, P. Peng, Z. Zheng, and H. Zhang, "Phosphorene quantum dot saturable absorbers for ultrafast fiber lasers," Sci. Rep. **7**, 42357 (2017).
10. K. Wu, B. Chen, X. Zhang, S. Zhang, C. Guo, C. Li, P. Xiao, J. Wang, L. Zhou, W. Zou, and J. Chen, "High-performance mode-locked and Q-switched fiber lasers based on novel 2D materials of topological insulators, transition metal dichalcogenides and black phosphorus: review and perspective (invited)," Opt. Commun. **406**, 214–229 (2018).
11. D. Hanlon, C. Backes, E. Doherty, C. S. Cucinotta, N. C. Berner, C. Boland, K. Lee, A. Harvey, P. Lynch, Z. Gholamvand, S. Zhang, K. Wang, G. Moynihan, A. Pokle, Q. M. Ramasse, N. McEvoy, W. J. Blau, J. Wang, G. Abellan, F. Hauke, A. Hirsch, S. Sanvito, D. D. O'Regan, G. S. Duesberg, V. Nicolosi, and J. N. Coleman, "Liquid exfoliation of solvent-stabilized few-layer black phosphorus for applications beyond electronics," Nat. Commun. **6**(1), 8563 (2015).
12. F. Xia, H. Wang, D. Xiao, M. Dubey, and A. Ramasubramaniam, "Two-dimensional material nanophotonics," Nat. Photonics **8**(12), 899–907 (2014).

#325231 https://doi.org/10.1364/OE.26.012506
Journal © 2018 Received 16 Mar 2018; revised 13 Apr 2018; accepted 15 Apr 2018; published 1 May 2018

Optics EXPRESS

13. Y. Chen, G. Jiang, S. Chen, Z. Guo, X. Yu, C. Zhao, H. Zhang, Q. Bao, S. Wen, D. Tang, and D. Fan, "Mechanically exfoliated black phosphorus as a new saturable absorber for both Q-switching and Mode-locking laser operation," Opt. Express **23**(10), 12823–12833 (2015).
14. J. Sotor, G. Sobon, M. Kowalczyk, W. Macherzynski, P. Paletko, and K. M. Abramski, "Ultrafast thulium-doped fiber laser mode locked with black phosphorus," Opt. Lett. **40**(16), 3885–3888 (2015).
15. H. Yu, X. Zheng, K. Yin, X. Cheng, and T. Jiang, "Thulium/holmium-doped fiber laser passively mode locked by black phosphorus nanoplatelets-based saturable absorber," Appl. Opt. **54**(34), 10290–10294 (2015).
16. M. Hisyam, M. Rusdi, A. Latiff, and S. Harun, "Generation of Mode-locked Ytterbium doped fiber ring laser using few-layer black phosphorus as a saturable absorber," IEEE J. Sel. Top. Quant. **23**(1), 1100205 (2016).
17. Z. Qin, G. Xie, C. Zhao, S. Wen, P. Yuan, and L. Qian, "Mid-infrared mode-locked pulse generation with multilayer black phosphorus as saturable absorber," Opt. Lett. **41**(1), 56–59 (2016).
18. Y. Chen, S. Chen, J. Liu, Y. Gao, and W. Zhang, "Sub-300 femtosecond soliton tunable fiber laser with all-anomalous dispersion passively mode locked by black phosphorus," Opt. Express **24**(12), 13316–13324 (2016).
19. J. Sotor, G. Sobon, W. Macherzynski, P. Paletko, and K. M. Abramski, "Black phosphorus saturable absorber for ultrashort pulse generation," Appl. Phys. Lett. **107**(5), 440–449 (2015).
20. Y. Q. Ge, S. Chen, Y. J. Xu, Z. L. He, Z. M. Liang, Y. X. Chen, Y. F. Song, D. Y. Fan, K. Zhang, and H. Zhang, "Few-layer selenium-doped black phosphorus: synthesis, nonlinear optical properties and ultrafast photonics applications," J. Mater. Chem. C Mater. Opt. Electron. Devices **5**(25), 6129–6135 (2017).
21. A. Favron, E. Gaufrès, F. Fossard, A.-L. Phaneuf-L'Heureux, N. Y. W. Tang, P. L. Lévesque, A. Loiseau, R. Leonelli, S. Francoeur, and R. Martel, "Photooxidation and quantum confinement effects in exfoliated black phosphorus," Nat. Mater. **14**(8), 826–832 (2015).
22. F. Torrisi, T. Hasan, W. Wu, Z. Sun, A. Lombardo, T. S. Kulmala, G.-W. Hsieh, S. Jung, F. Bonaccorso, P. J. Paul, D. Chu, and A. C. Ferrari, "Inkjet-printed graphene electronics," ACS Nano **6**(4), 2992–3006 (2012).
23. I. M. Hutchings and G. D. Martin, *Inkjet Technology for Digital Fabrication* (John Wiley & Sons, Ltd., 2012).
24. G. L. Robertson, *Food packaging: principles and practice* (CRC, 2012).
25. S. Santra, G. Hu, R. C. T. Howe, A. De Luca, S. Z. Ali, F. Udrea, J. W. Gardner, S. K. Ray, P. K. Guha, and T. Hasan, "CMOS integration of inkjet-printed graphene for humidity sensing," Sci. Rep. **5**(1), 17374 (2015).
26. G. Hu, J. Kang, L. W. T. Ng, X. Zhu, R. C. T. Howe, C. Jones, M. C. Hersam, and T. Hasan, "Functional inks and printing of two-dimensional materials," Chem. Soc. Rev. in press.
27. R. D. Deegan, O. Bakajin, T. F. Dupont, G. Huber, S. R. Nagel, and T. A. Witten, "Capillary flow as the cause of ring stains from dried liquid drops," Nature **389**(6653), 827–829 (1997).
28. T. Hasan, Z. Sun, F. Wang, F. Bonaccorso, P. H. Tan, A. G. Rozhin, and A. C. Ferrari, "Nanotube–polymer composites for ultrafast photonics," Adv. Mater. **21**(38–39), 3874–3899 (2009).
29. J. R. Brent, N. Savjani, E. A. Lewis, S. J. Haigh, D. J. Lewis, and P. O'Brien, "Production of few-layer phosphorene by liquid exfoliation of black phosphorus," Chem. Commun. (Camb.) **50**(87), 13338–13341 (2014).
30. D. Mao and H. Lu, "Formation and evolution of passively mode-locked fiber soliton lasers operating in a dual-wavelength regime," J. Opt. Soc. Am. B **29**(10), 2819–2826 (2012).
31. X. Zhao, Z. Zheng, L. Liu, Q. Wang, H. Chen, and J. Liu, "Fast, long-scan-range pump-probe measurement based on asynchronous sampling using a dual-wavelength mode-locked fiber laser," Opt. Express **20**(23), 25584–25589 (2012).
32. G. P. Agrawal, *Nonlinear Fiber Optics* (Academic, 1995).
33. C. Spielmann, P. F. Curley, T. Brabec, and F. Krausz, "Ultrabroadband femtosecond lasers," IEEE. J. Quantum Electron. **30**(4), 1100–1114 (1994).
34. D. Y. Tang, L. M. Zhao, B. Zhao, and A. Q. Liu, "Mechanism of multisoliton formation and soliton energy quantization in passively mode-locked fiber lasers," Phys. Rev. A **72**(4), 043816 (2005).

1. Introduction

Passively mode-locked fiber laser sources are now established as a common tool for femtosecond pulse generation at MHz repetition rates. The ever-growing demands from laser end-users for shorter pulse duration and more versatile pulse sources are driving the community to seek new laser designs, aiming to broaden the parameter space such devices can achieve. It is widely accepted that the formation of the pulses and their steady-state characteristics are strongly dependent on the cavity dispersion and nonlinearity, in addition to the contributions from the spectral filtering effect of a finite gain bandwidth, gain saturation and loss. For instance, in soliton fiber lasers, the practically achievable pulse duration is typically limited to ~200 fs as the pulse duration (τ) of fundamental solitons has to satisfy $\tau > \sqrt{|\beta_2| L}$, where β_2 is the group velocity dispersion (GVD), and L is the cavity length [1]. With a typical GVD of –22 ps^2/km at 1.55 μm, 100 fs pulse would require 45 cm long cavity. For such short L, it is not easy to compensate the dispersion and nonlinearity. Achieving ~100 fs pulses is therefore very challenging. To circumvent this limitation, in 1993, Tamura *et al.*

Optics EXPRESS

proposed *stretched-pulse laser* [1], where the net cavity dispersion was designed to be close to zero. By including segments of normally and anomalously dispersive fiber, the pulse in this cavity experienced periodic broadening and compression in each round trip. The cavity could therefore tolerate a larger nonlinear phase shift than a soliton laser, leading to a significant reduction in the achievable pulse duration at specific output positions.

While a large number of studies have reported stretched pulse fiber lasers using saturable absorbers (SAs) [2–5], two-dimensional (2D) nanomaterials (e.g. graphene [6,7], semiconducting transition metal dichalcogenides (s-TMDs) [8] and black phosphorus (BP) [9,10]) are often preferred as they offer strong intensity-dependent absorption, broadband working wavelength range, ultrafast carrier dynamics, in addition to the ease of all-fiber integration. In comparison to graphene and s-TMDs, BP is of particular interest due to its unique band structures [11, 12]. BP has been shown to exhibit a layer-dependent bandgap, varying from 0.3 eV (bulk) to 2 eV (monolayer), bridging the gap between zero-gap graphene and large-gap s-TMDs. Most recently, a growing number of studies have reported BP-based femtosecond fiber lasers, with operating range covering from 1 to 2.8 μm either at discrete wavelength or with broadband tunability [13–18]. Examples of experimental studies exploiting the saturable absorption properties of BP include demonstrations of 272 fs pulses with 10.2 nm bandwidth and 516 fs with 12.5 bandwidth in erbium-doped (Er-doped) fiber lasers [19, 20]. These are the shortest pulse duration and the broadest bandwidth demonstrated directly from a fiber oscillator mode-locked by BP-based SAs to date. However, due to BP degradation at ambient conditions [21], the optoelectronic and photonic device fabrication using BP has been prevalently limited to mechanically exfoliated BP under protective atmospheres. Scalable fabrication of BP SAs with long-term operation stability in the ambient remains a key target for the successful use of this novel material.

In this manuscript, we report an ultrafast stretched pulse fiber laser integrating inkjet-printed BP-based SA fabricated from functional ink of liquid-phase-exfoliated BP. Through intracavity dispersion management, the BP SA based cavity generates 102 fs pulses with 40 nm spectral width, both of which are ~3 times shorter and wider than previous reports, respectively. Through a single step, pin-hole free encapsulation process, the SA device also achieves long- term ambient stability against degradation, demonstrating a self-starting mode-locking operation stable for >10 days without any noticeable performance degradation. We further provide numerical simulations of the pulse and spectrum evolution along the cavity, which are in good agreement with our experimental results. Our work highlights the applicability of BP-based devices for photonic applications requiring stable femtosecond pulse generation under ambient conditions.

2. BP SA fabrication and characterization

To fabricate the BP SA, we first produce few layer BP flakes via ultrasound assisted liquid phase exfoliation. For this, 10 mg bulk BP crystals (Smart Elements) are bath-sonicated in 10 mL anhydrous N-methyl-2-pyrrolidone under nitrogen for 12 h at 15 °C. After centrifugation at 1500 × *g* for 30 min, the resultant dispersion [Fig. 1(a)] contains exfoliated BP flakes with an average thickness of 3.37 nm, equivalent to ~6 layers [Fig. 1(b)]. For ink formulation, the BP flakes are solvent-exchanged into anhydrous isopropanol through iterative centrifugation; 10 vol.% anhydrous 2-butanol is then added to yield a highly-concentrated BP ink (~5 gL^{-1}) with a viscosity of 2.2 mPas, a surface tension of 28 mNm^{-1}, and a density of 0.8 gcm^{-3}. With 22 μm nozzle (Fujifilm DMC-11610) used in this work, the BP ink gives an inverse Ohnesorge number of ~10, ensuring a stable inkjet printing [22, 23]. This low ink surface tension also guarantees adequate wetting of commonly used conformable and rigid substrates (e.g. Si/SiO_2, glass and polyethylene terephthalate (PET) [24–26]). This binary solvent ink composition also induces recirculating Marangoni flows to redistribute the suspended BP flakes during the ink drying process, suppressing the formation of ‘coffee rings’ (i.e. ring like material deposition at the edges of drying droplets [26, 27]) for a spatially uniform deposition

Optics EXPRESS

[Figs. 1(c) and 1(d)] on nonporous substrates. This is of critical importance for stable, reproducible operation of inkjet-printed-BP-based devices.

We then fabricate the SA by inkjet printing the binary solvent based functional BP ink onto an ultrathin (1.5 μm) PET substrate, followed by encapsulation with a 100 nm thick pin-hole free Parylene-C passivation layer. The intensity-dependent absorption of the fabricated BP SA (i.e. two pieces of films stacked together) at 1.55 μm is investigated using open-aperture Z-scan [28]. The sample is swept through the focal plane of a beam of ultrashort pulses (150 fs pulse duration, 1562 nm wavelength, 10 MHz pulse repetition frequency), while the transmitted power through SA is recorded against a reference power. With increasing peak intensity, the material absorption decreases, confirming saturable absorption. A typical data set from a single Z-scan measurement, at a fixed transverse position on the sample, can be well-fitted in a two-level SA model,

$$\alpha(I) = \alpha_0 / (1 + I/I_{sat}) + \alpha_{ns} \quad (1)$$

where I is the intensity of the input optical pulse, α is the intensity-dependent absorption, giving a modulation depth α_0 ~10.03%, non-saturation absorption α_{ns} ~9.97% and a saturation intensity I_{sat} ~14.98 MW/cm^2 [Fig. 2]. Such SA parameters are similar in magnitude to previously reported SAs based on BP [13–18].

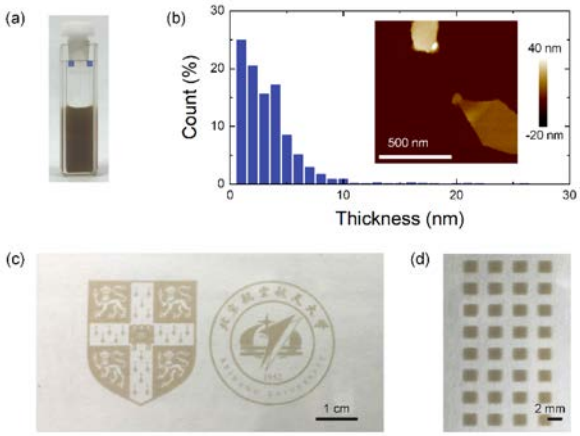

Fig. 1. (a) Photograph of the as produced BP dispersion. (b) Atomic force microscopy (AFM) thickness histogram of the exfoliated BP fakes, showing the flakes are 3.37 nm thick on average, equivalent to ~6 layers (0.9 nm for the first single layer and 0.5 nm for subsequent individual layers [29]). Inset: AFM micrograph of selected exfoliated BP fakes. (c) Inkjet-printed large-scale BP patterns on PET showing university crests, and (d) inkjet-printed BP SA arrays, showing spatially uniform printed SA devices.

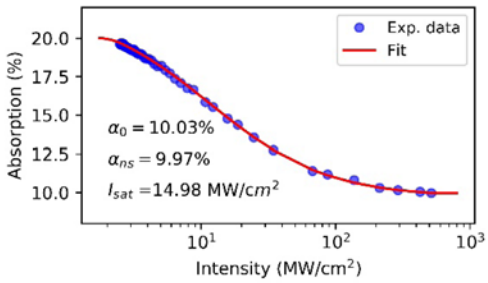

Fig. 2. A typical data set from Z-scan experiment of the SA device.

Optics EXPRESS

3. Experimental setup and results

We construct an Er-doped fiber laser, using a travelling wave ring cavity design combined with a dispersion management approach to generate ultrashort (100 fs or sub-100 fs) pulses [Fig. 3]. To achieve this, the BP SA is inserted into a fiber laser by sandwiching two ~1 mm × 1 mm pieces between two fiber connectors. The Er-doped fiber amplifier consists of a length of 4.05 m single-mode Er-doped fiber (YOFC, EDF1007, with an estimated GVD of 24 ps^2/km at 1.55 μm. This is calculated using the dispersion measurement of an asynchronously dual-wavelength mode-locked fiber laser [30, 31]), co-pumped by a 980 nm laser diode through a 0.9 m fused 980/1550 wavelength division multiplexer (WDM, where its pigtail consists a piece of HI1060 fiber with a GVD of –7 ps^2/km at 1.55 μm). In addition to the fiber amplifier, the cavity consists of a 20: 80 fiber-pigtailed optical output coupler (OC) for both spectral and temporal diagnostics, a polarization-independent inline fiber isolator to ensure unidirectional propagation and a polarization controller, all of which is made of single-mode fiber (SMF) with a GVD of –22 ps^2/km. The entire length of the ring cavity is 8.60 m and the net cavity dispersion is estimated as –0.01 ps^2.

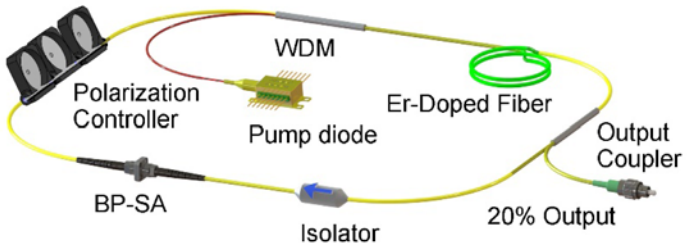

Fig. 3. Experimental setup of the stretched-pulse fiber laser. WDM, wavelength-division multiplexer. BP-SA, black phosphorus saturable absorber.

Self-starting mode-locking is observed at the fundamental repetition frequency of cavity of 23.9 MHz (a corresponding time interval of 41.9 ns [Fig. 4(a)]), with 1.7 mW output power (corresponding to a single pulse energy of 71 pJ), at a pump power of 34 mW. Figure 4(b) shows the optical spectrum of the generated pulses, centered at 1555 nm, with a full-width at half maximum (FWHM) of 40 nm, corresponding to a transform-limit pulse duration of 88 fs in a Gaussian pulse shape. The autocorrelation trace, measured using an intensity autocorrelator, is well-fitted by a Gaussian profile, showing a deconvolved pulse duration of 102 fs [Fig. 4(c)]. The time-bandwidth product is 0.51, indicating that the cavity has a low chirp. This could be attributed to the uncompensated high order dispersion [32, 33]. The fundamental radio frequency spectrum, measured on a span of 500 kHz, shows a signal-to-background contrast of >60 dB, indicating good mode-locking performance of the cavity [Fig. 4(d)]. The long-term stability of the BP-based SA device and mode-locking performance are further evaluated by recording the optical spectra of the laser emission every 4 hours for > 240 hours under a fixed experimental condition. No significant degradation of optical spectra profile (i.e. central wavelength and spectral width) is observed along the measurement period, as shown in Figs. 4(e) and 4(f). This demonstrates that the mode-locking operation possesses a good operation performance against BP degradation at ambient conditions. We note that the device can potentially operate for much longer as the performance of the laser remained unchanged when we terminated the measurement.

Optics EXPRESS

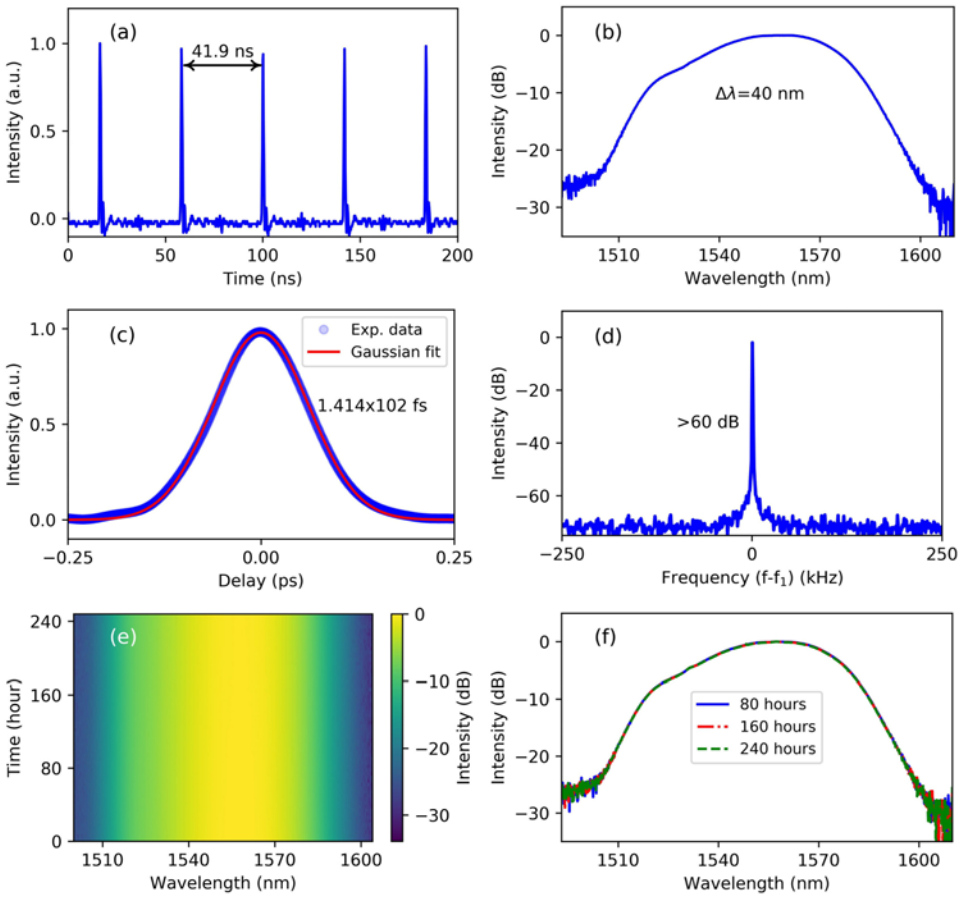

Fig. 4. (a) Oscilloscope trace of the laser output. (b) Optical spectrum with a bandwidth of 40 nm. (c) Autocorrelation trace with a Gaussian fit. (d) Radio frequency spectrum, on a 500 kHz range span, with a 30 Hz resolution, measured around the fundamental repetition rate f1 = 23.9 MHz. (e) Spectra of long-term stable operation over 240 hours. (f) Spectra acquired after 80 hours (blue curve), 160 hours (red dot line), and 240 hours (green dot line), respectively.

4. Numerical simulation

To gain further insight into the dynamics of our stretched-pulse fiber cavity, we perform numerical simulations based on a modified nonlinear Schrödinger equation (NLSE) [34]:

$$\frac{\partial U}{\partial Z} = -i\frac{\beta_2}{2}\frac{\partial^2 U}{\partial t^2} + i\gamma|U|^2 U + \frac{g}{2}U + \frac{g}{2\Omega_g}\frac{\partial^2 U}{\partial t^2} \tag{2}$$

where U is the envelope of the field, β_2 is the GVD parameter, Z is the propagation distance, t is the physical time, γ is the nonlinear parameter, and Ω_g is the gain bandwidth. The laser gain g is given by

$$g = G\exp(-P_{ave}/P_{sat}) \tag{3}$$

where G is the small signal gain coefficient, P_{sat} is the gain saturation power, and P_{ave} is the average power. The intensity discrimination, necessary for promoting mode-locking (SA), acts as a small perturbation to the NLSE and is expressed by Eq. (1). The simulated parameters of optical devices included in the numerical model are summarized in Table 1.

Optics EXPRESS

Table 1. Fiber Parameters of the Numerical Simulations

EDF	SMF	HI1060	OC	BP-SA
β_2 = 24 ps^2/km γ = 5 W^{-1}km^{-1} L = 4.05 m; P_{sat} = 1.43mW G = 0.69; Ω_g = 40 nm	β_2 = –22 ps^2/km γ = 1.1 W^{-1}km^{-1} L = 3.65 m	β_2 = –7 ps^2/km γ = 1.5 W^{-1}km^{-1} L = 0.9 m	20% output	α_0 = 10.03% α_{ns} = 9.97% P_{sat} = 13.3 W

Starting from the amplifier, the simulation enables the temporal and spectral dynamics in the steady-state to be visualized on a single round-trip of the cavity. The co-action of the GVD and self-phase modulation (SPM) leads to the pulse breathing twice [Fig. 5(a)], while the spectrum breathing once in one round-trip [Fig. 5(b)]. The breathing ratio of temporal and spectral widths of the pulse is calculated to be 20.4 and 4.7, respectively. We note that the OC is placed at the position before the intra-cavity pulse becomes shortest. The pulse taken directly at the OC has a duration of 1.02 ps with an up-chirp, indicated by the pulse profile and its spectrogram; Fig. 5(c). This allows the pulse to be further compressed by a length of external fiber with anomalous dispersion (fiber pigtail of the OC). The optimal length of fiber pigtail of the OC in the simulation is 1.2 m, in accordance with parameters used in our experiment, resulting in a nearly chirp-free pulse, with a duration of 105 fs [Fig. 5(d)]. We conclude that the simulated results are in a good agreement with experimental results for similar output energies, pulse durations and spectral FWHMs: 73 pJ and 71 pJ, 105 fs and 102 fs, and 43.2 nm and 40 nm for simulation and experiment, respectively.

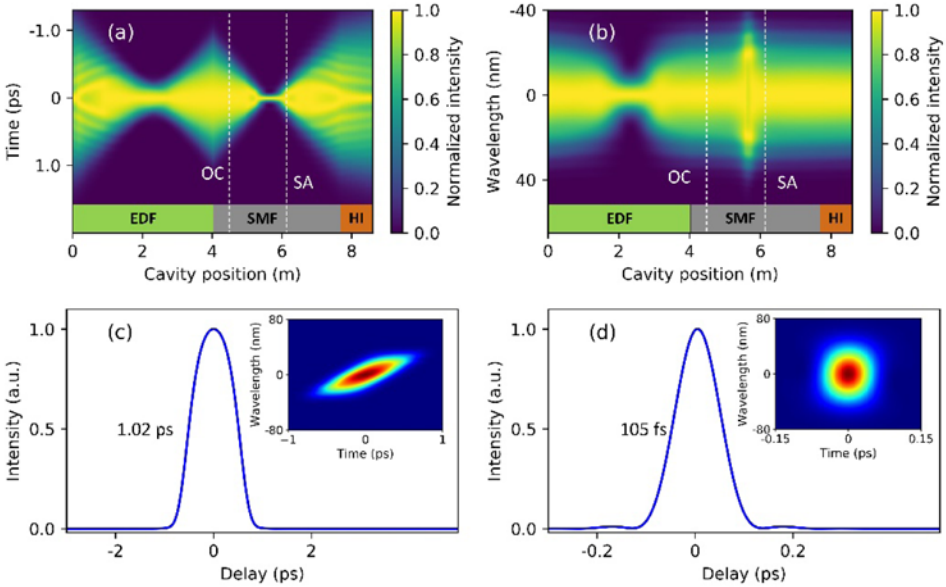

Fig. 5. Simulation results of (a) temporal pulse evolution, (b) spectrum evolution against the position in the cavity. Output pulse profile propagating through (c) 0 m and (d) 1.20 m of the fiber-pigtailed OC. Insets show the corresponding spectrograms.

5. Conclusion

In summary, we have demonstrated a long-term stable, stretched-pulse Er-doped fiber laser with 102 fs duration and 40 nm spectral width, mode-locked using an inkjet-printed BP SA. The laser design enabled the shortest pulses achievable with the broadest bandwidth to date, directly from an inkjet-printed BP-based mode-locked fiber laser, constituting 2.7 times improvement in pulse duration and 3.2 times in spectral bandwidth compared to previous reports. Our simple all-fiber design and scalable fabrication strategy promotes towards the

Optics EXPRESS

development of utilizing 2D materials to generate long-term reliable mode-locking in a small footprint, suitable for packing in a compact single-unit laser system for applications requiring ultrashort pulses with broad bandwidth.

Funding

EPSRC (EP/L016087/1, EP/G037221/1); Fundamental Research Funds for the Central Universities and NSFC (61505005/51778030).

131.111.184.102 {ts '2018-07-20 09:02:24'}